



Magnetic fields of BigRIPS magnet

H. Takeda

BigRIPS Team, RIKEN Nishina Center

BigRIPS Analysis Workshop

2014/9/11



Contents

-- *How field maps are analyzed and used in ion-optical calculation (COSY) --*

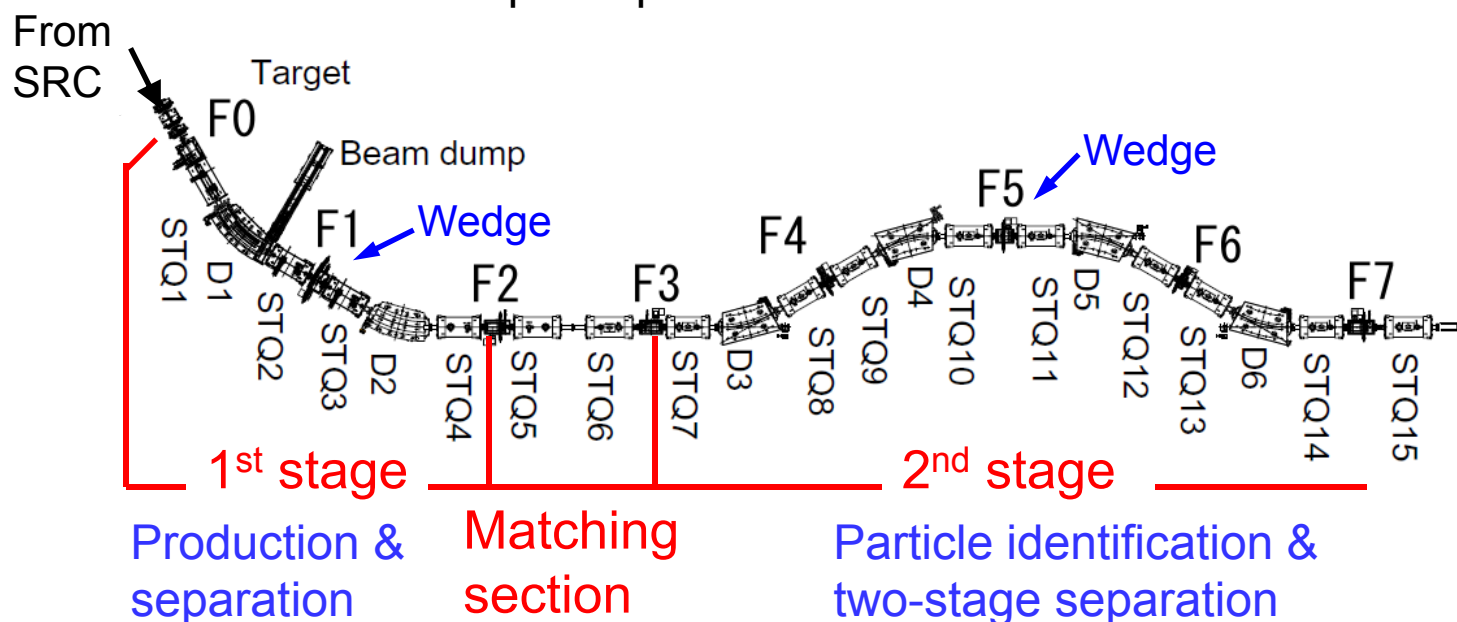
- Introduction
- Field map analysis
 - Surface map analysis of quadrupoles
 - Dipoles
- Examples of ion-optical calculation
- Summary



Features of BigRIPS magnet

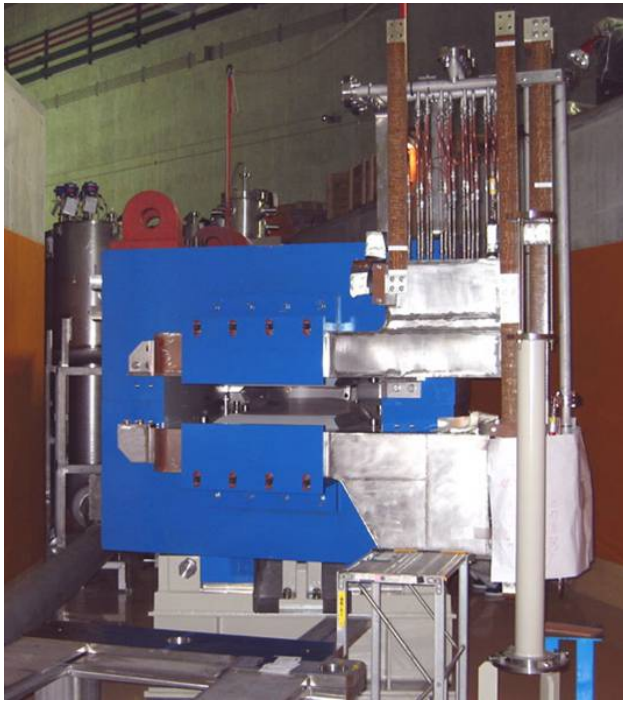
For efficient transmission of RI beams even when the in-flight fission of uranium beams is employed as a production reaction, BigRIPS magnets have following features:

- 1) **Large acceptances**
 - Comparable with angular / momentum spreads of **in-flight fission** at RIBF energy (± 50 mrad, $\pm 5\%$)
- 2) **Superconducting quads** with a **large aperture**, and **strong field**
 - Pole tip radius: 170 mm
 - Maximum pole tip field: 2.4 T



Parameters:
 $\Delta a = \pm 40$ mrad
 $\Delta b = \pm 50$ mrad
 $\Delta p/p = \pm 3\%$
 $B_p = 9$ Tm
 $L \sim 78$ m

Room-temperature Dipole (D1-D6)

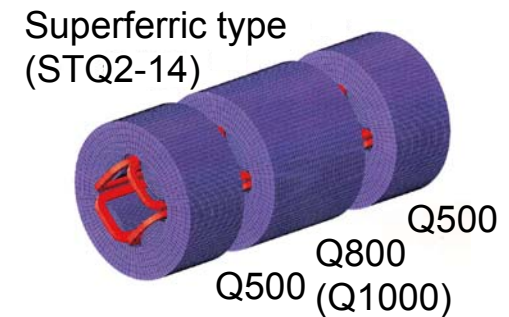
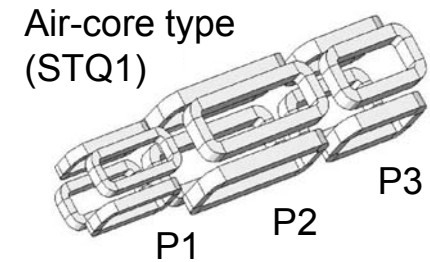


H-type, $\rho=6$ m, 30deg bend
 pole gap=140 mm
 weight=56 tons
 maximum field=1.75 T (10.5Tm)

Superconducting triplet quadrupole and sextupole (STQ1-14)



pole tip radius=170 mm
 bore radius=120 mm
 (90mm for STQ1-P1)
 effective length
 ~500mm (STQ1-P1/3,Q500)
 ~800mm (STQ1-P2,Q800)
 ~1000mm (Q1000)
 maximum field gradient
 24T/m for STQ1-P1
 20T/m for STQ1-P2,3
 14.1T/m for STQ2-14



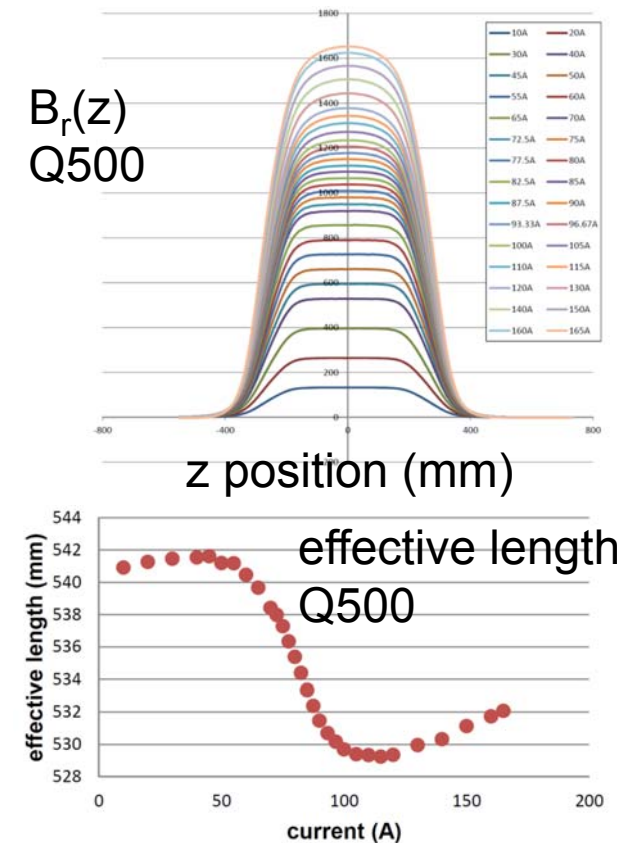
Sextupole magnet is superimposed on one of the Q500 magnet



Our goal: accurate ion-optical setting *without any tuning*

Various problems concerning
short-length, large-aperture, and strong field magnets.

- **Large fringing field region**
 - Entire region must be treated as fringe.
 - **Large saturation effect**
 - Shape and effective length vary drastically with the magnet excitation.
 - **Existence of pseudo terms**
 - originate from the changes of the magnetic field along the beam axis
- The effects of the varying field maps should be included in the ion-optical simulation.





Surface map analysis of 3D magnetic field

obtained by solving Laplace's eq. in cylindrical coordinate system

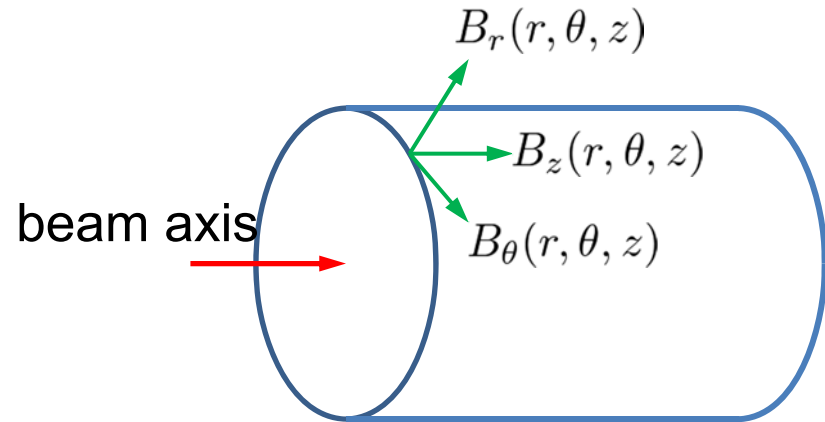
$$(\vec{\nabla}^2 \Phi = 0, \text{ where } \vec{B} = \vec{\nabla} \Phi)$$

see Takeda et al., NIM B317 (2013) 798

surface measurement

Fourier analysis

$$\begin{cases} B_r(r, \theta, z) = \sum_{n=1}^{\infty} B_{r,n}(r, z) \sin n\theta, \\ B_\theta(r, \theta, z) = \sum_{n=1}^{\infty} B_{\theta,n}(r, z) \cos n\theta, \\ B_z(r, \theta, z) = \sum_{n=1}^{\infty} B_{z,n}(r, z) \sin n\theta. \end{cases}$$



Extraction of $b_{n,0}$

(without skew terms for simplicity)

$$\begin{cases} B_{r,n}(r, z) \equiv \left(\frac{r}{r_0}\right)^{n-1} \sum_{m=0}^{\infty} b_{n,m}(z) \left(\frac{r}{r_0}\right)^{2m}, \\ B_{\theta,n}(r, z) \equiv \left(\frac{r}{r_0}\right)^{n-1} \sum_{m=0}^{\infty} \frac{n}{n+2m} b_{n,m}(z) \left(\frac{r}{r_0}\right)^{2m}, \\ B_{z,n}(r, z) \equiv \left(\frac{r}{r_0}\right)^n \sum_{m=0}^{\infty} \frac{r_0}{n+2m} \frac{\partial}{\partial z} b_{n,m}(z) \left(\frac{r}{r_0}\right)^{2m}. \end{cases}$$

3D magnetic field (B_r , B_θ , B_z) is expressed by $b_{n,0}(z)$ only.

It can be extracted from measured surface map.

$$b_{n,m}(z) = -\frac{r_0^2}{4m(n+m)} \frac{n+2m}{n+2(m-1)} \frac{\partial^2}{\partial z^2} b_{n,m-1}(z).$$

($b_{n,0}$: leading term, $b_{n,m>0}$: pseudo terms)

Advantages of this method

- **only one component (B_r or B_θ) is sufficient**
- **$b_{n,0}(z)$ depends only on z**
 - 3D field map which satisfies Maxwell's eq. is obtained by $b_{n,0}(z)$ function
 - easy to parameterize full 3D map
 - desirable for ion-optical calculation (COSY)
- **Measurement errors are averaged during the integration process of Fourier transform**

(cf. traditional surface data method)

based on Helmholtz's theorem

$$\vec{B}(\vec{x}) = \vec{\nabla} \phi(\vec{x}) + \vec{\nabla} \times \vec{A}(\vec{x})$$

where

$$\phi(\vec{x}) = \int_{\partial V} \frac{\hat{n}(\vec{x}') \cdot \vec{B}(\vec{x}')}{4\pi |\vec{x} - \vec{x}'|} dS - \int_V \frac{\vec{\nabla} \cdot \vec{B}(\vec{x}')}{4\pi |\vec{x} - \vec{x}'|} dV$$

$$\vec{A}(\vec{x}) = \int_{\partial V} \frac{\hat{n}(\vec{x}') \times \vec{B}(\vec{x}')}{4\pi |\vec{x} - \vec{x}'|} dS + \int_V \frac{\vec{\nabla} \times \vec{B}(\vec{x}')}{4\pi |\vec{x} - \vec{x}'|} dV$$

in the case of $\nabla \cdot \vec{B} = \nabla \times \vec{B} = 0$

⇒ volume integral term=0

3D field map is described by surface data.
shape of the surface is arbitrary.

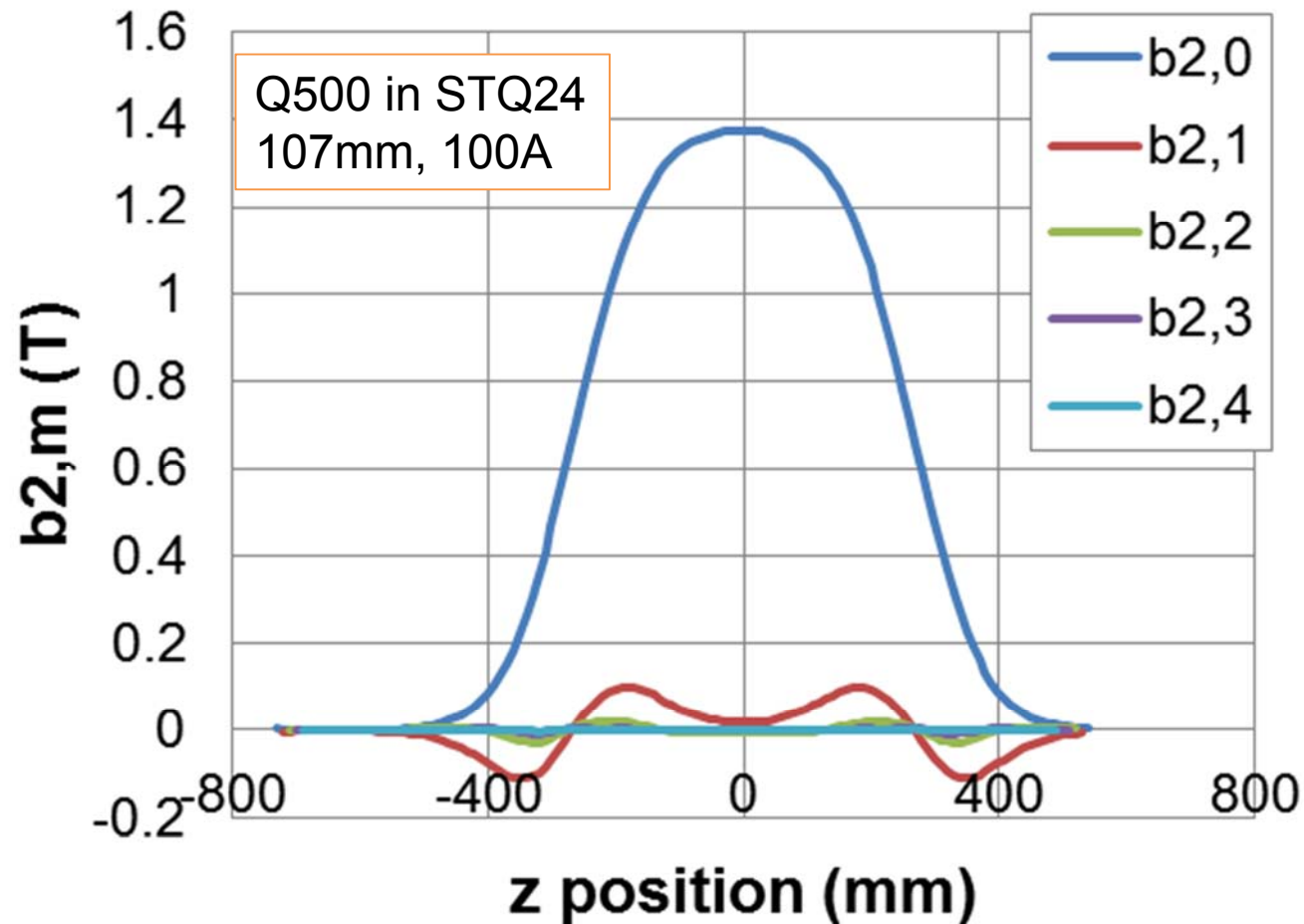
all the three components are necessary.



Our method

cylinder shape
only one component
is sufficient

extracted $b_{2,0\sim4}$



ratio to $b_{2,0}$

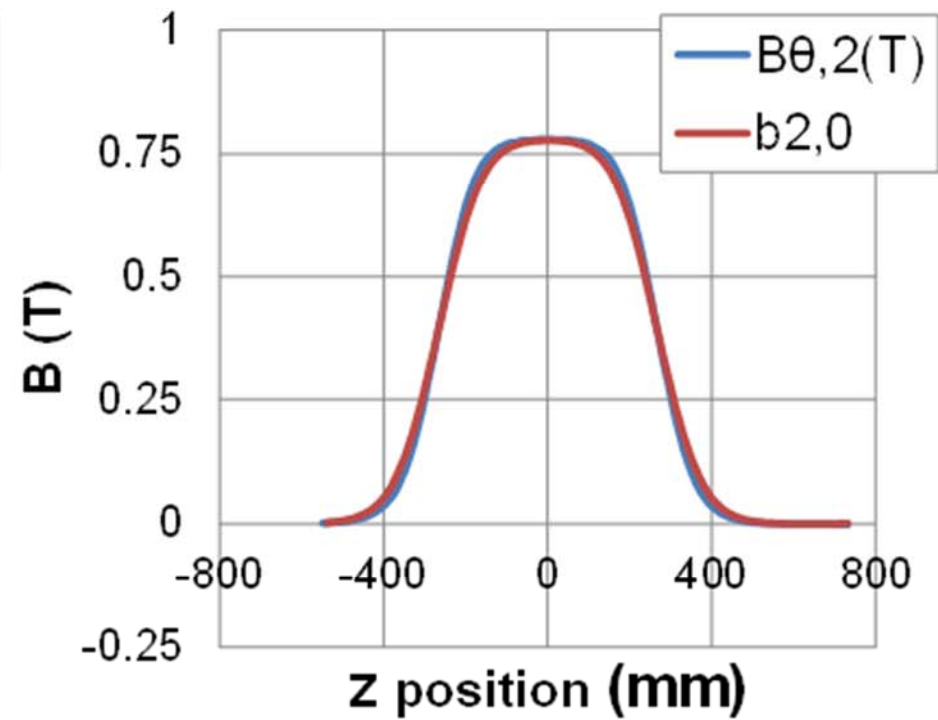
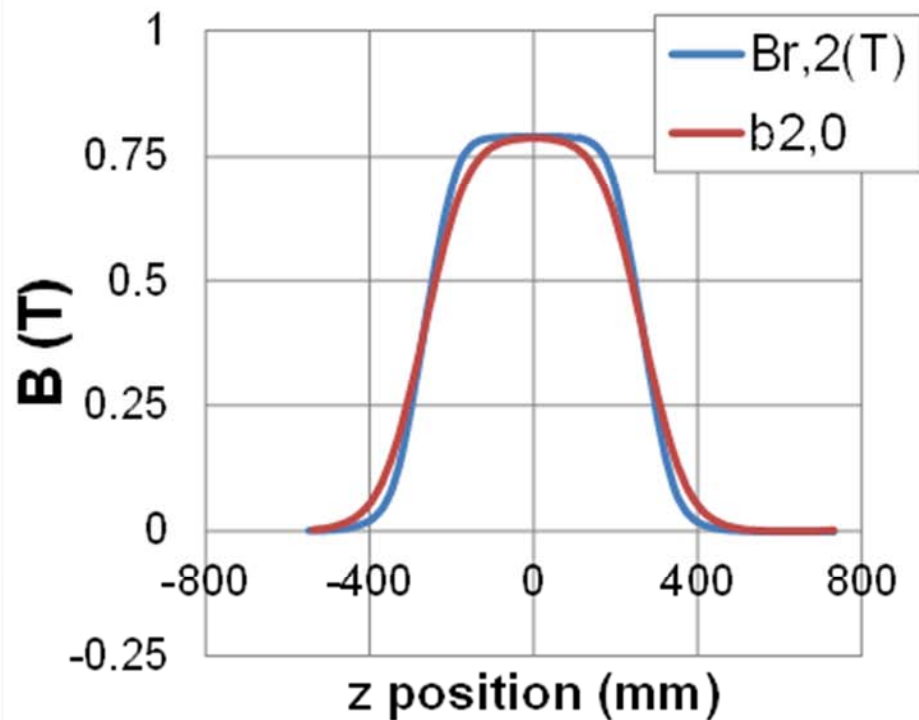
- $b_{2,1} \dots 7 \sim 8\%$
- $b_{2,2} \dots 1 \sim 2\%$
- $b_{2,3} \dots 0.3 \sim 0.5\%$
- $b_{2,4} \dots 0.1 \sim 0.2\%$

$$b_{n,m}(z) = -\frac{r_0^2}{4m(n+m)} \frac{n+2m}{n+2(m-1)} \frac{\partial^2}{\partial z^2} b_{n,m-1}(z).$$

Comparison between $B_{r,2}$, $B_{\theta,2}$ and $b_{2,0}$

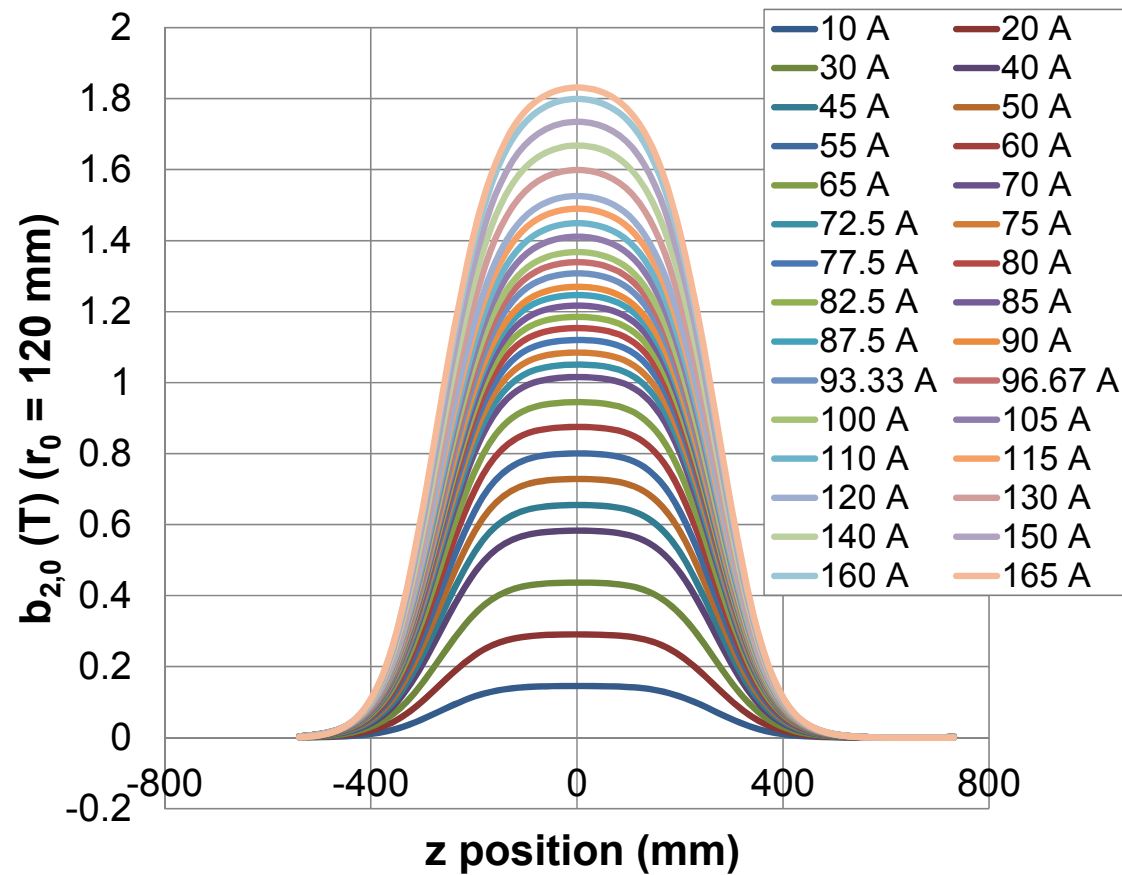
$$B_{r,2}(r, z) = b_{2,0}(z) \left(\frac{r}{r_0}\right) + b_{2,1}(z) \left(\frac{r}{r_0}\right)^3 + b_{2,2}(z) \left(\frac{r}{r_0}\right)^5 + \dots$$

$$B_{\theta,2}(r, z) = b_{2,0}(z) \left(\frac{r}{r_0}\right) + \frac{2}{2+2} b_{2,1}(z) \left(\frac{r}{r_0}\right)^3 + \frac{2}{2+4} b_{2,2}(z) \left(\frac{r}{r_0}\right)^5 + \dots$$



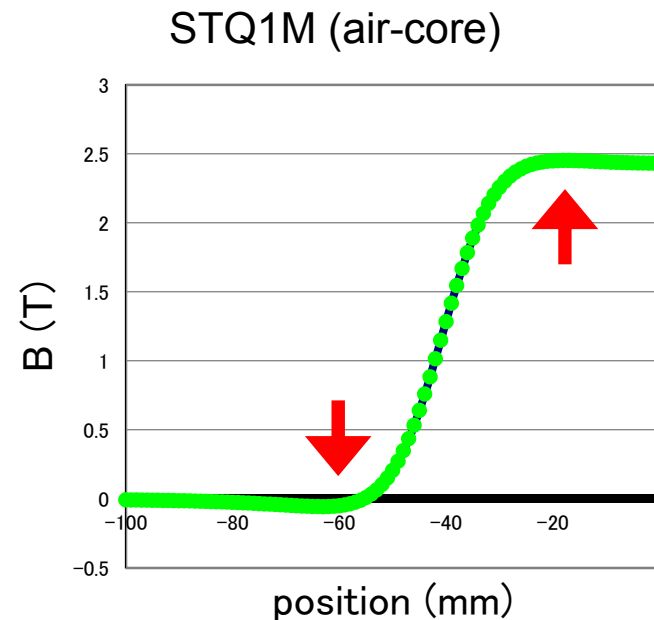
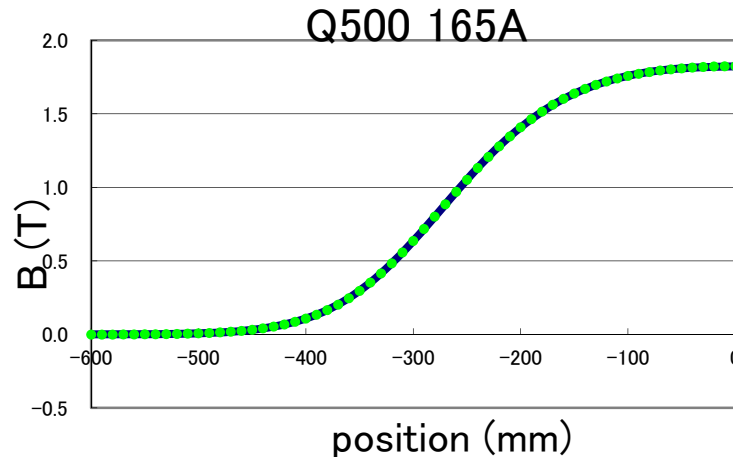
Q500 in STQ24, 107mm, 60A

$b_{2,0}$ at different excitation currents



Fringing field fitting

Enge coefficients a_i are freely searched to minimize $\sum_i [b_{2,0}(z_i) - \text{Enge}(z_i)]^2$.



$$F(z) = \frac{1}{1 + \exp[a_1 + a_2(z/D) + \dots + a_6(z/D)^5]}$$

(D : full aperture)

Folded expression

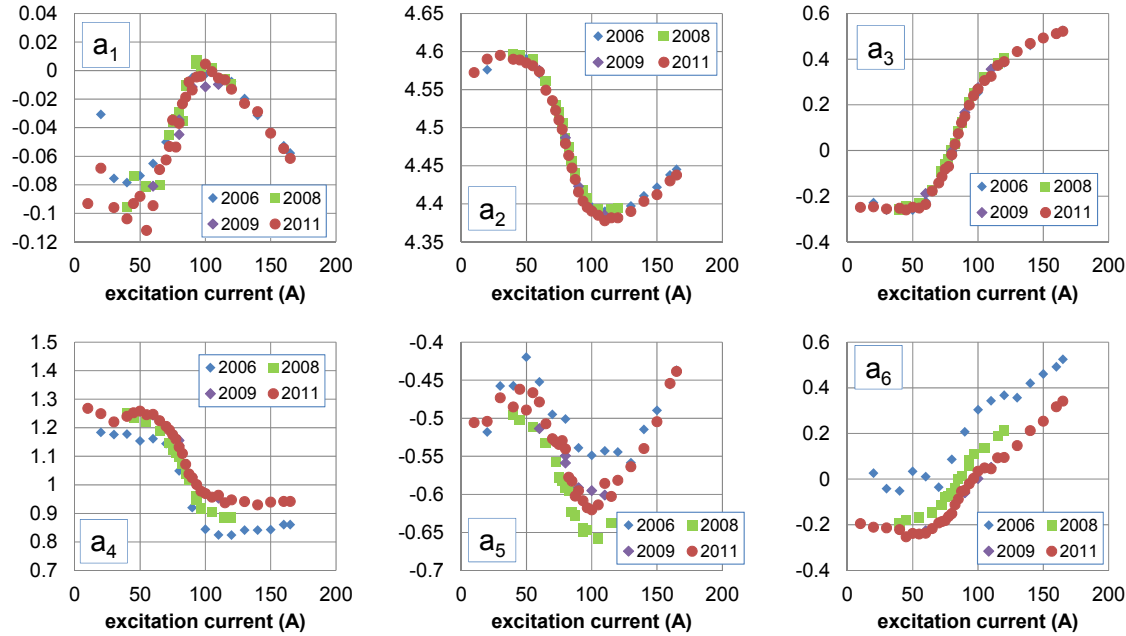
$$b_{2,0}(z) = B_c \cdot F_{in} \cdot F_{out}$$

→ implemented in COSY

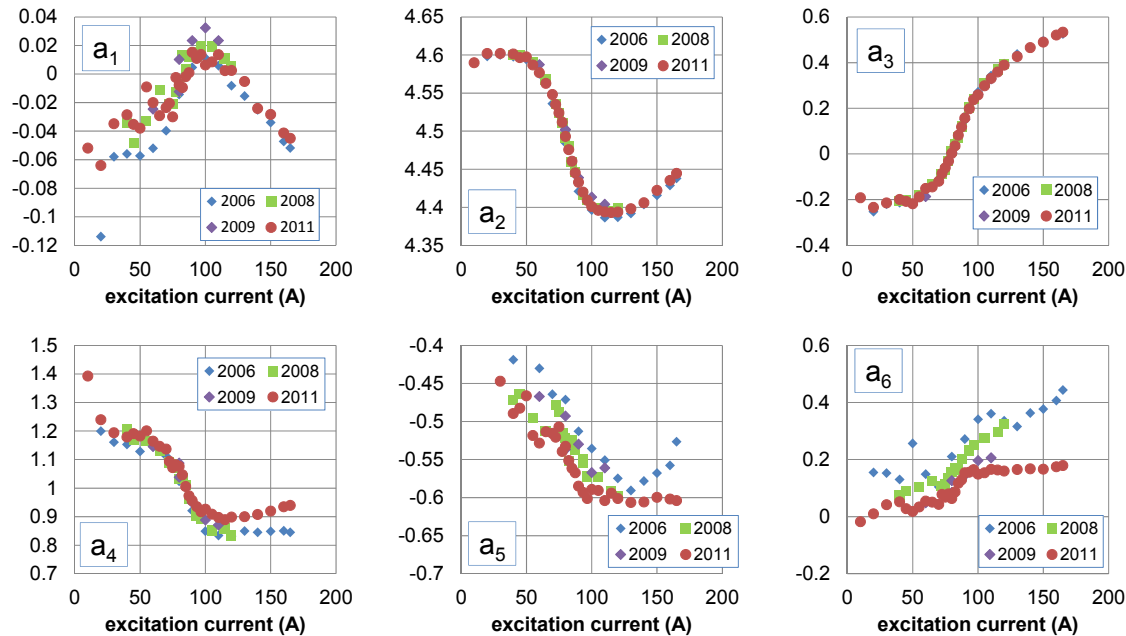
$$F(z) = \frac{1}{1 + \exp[a_1 + a_2(z/D) + \dots + a_6(z/D)^5]} + a_7 \tanh(a_8 + a_9(z/D)) \cdot \exp\left[-\left(\frac{z/D + a_{10}}{a_{11}}\right)^2\right]$$

Second term is introduced to express under- & overshooting shaped fields.

Q500 entry side



Q500 exit side



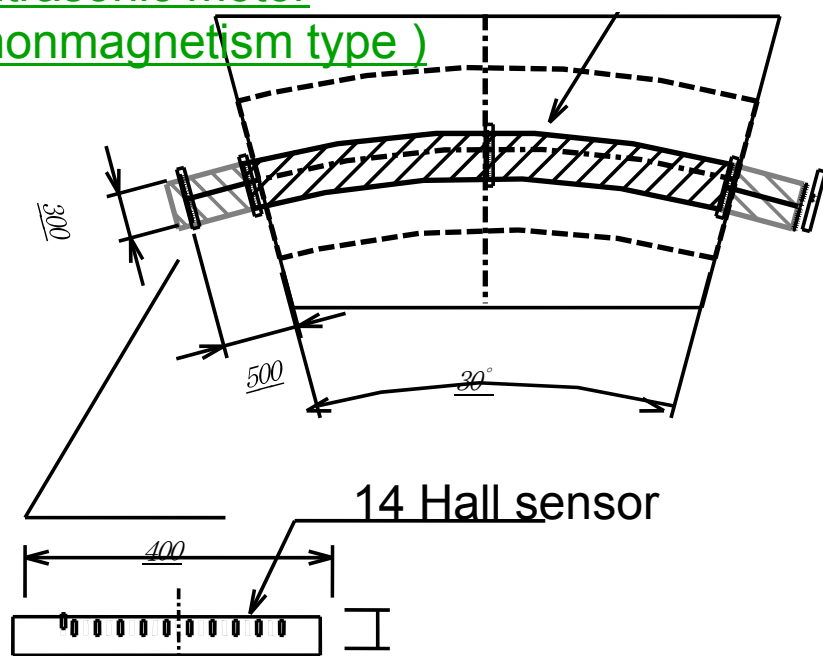
$b_{2,0}$ at any excitation current can be obtained by interpolating these Enge coefficients.



Magnetic field measurement for Dipole magnet

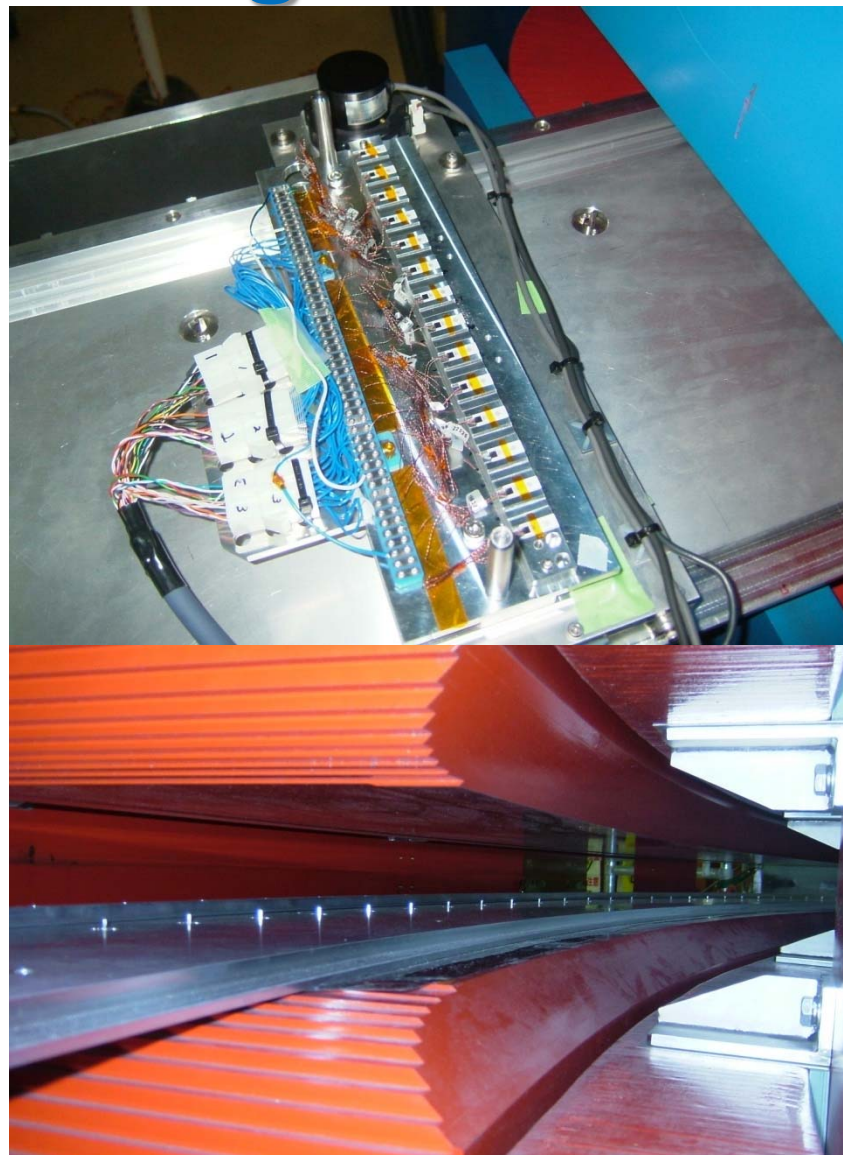
Running gear
(ultrasonic motor
nonmagnetism type)

R6000, 30 degree.



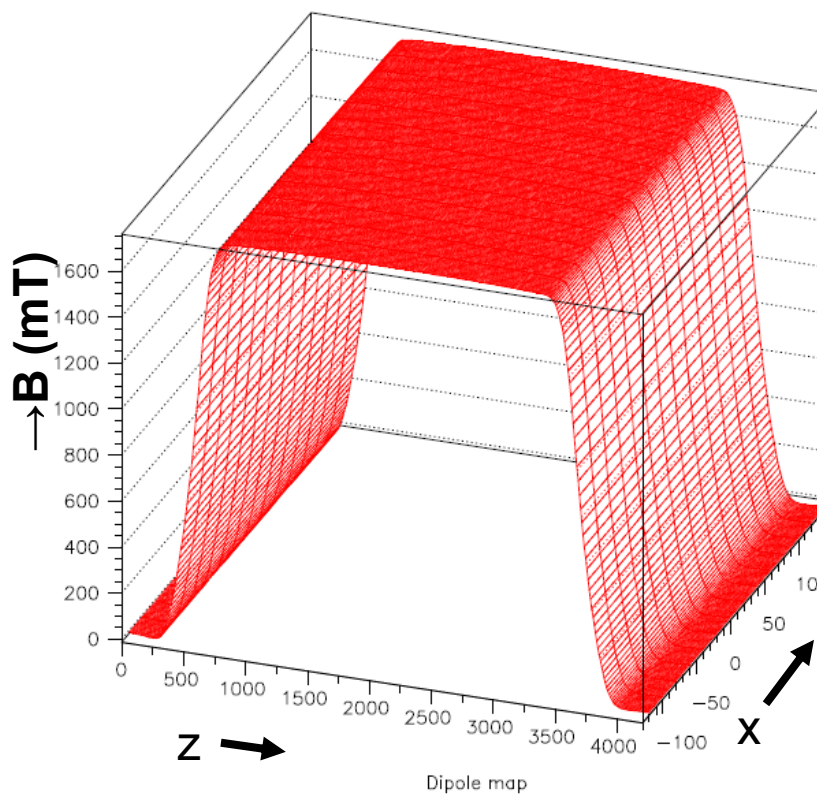
Measurement range : size of dipole $\pm 500\text{mm}$
Interval of cross direction : 20mm (center 10mm)
Measurement plane : center, $\pm 10\text{mm}$, 20mm ,
(Gap $\pm 70\text{mm}$) 30mm . 40mm
Measurement Magnetic field
 100A to 1100A interval to 100A

(by Y. Yanagisawa)



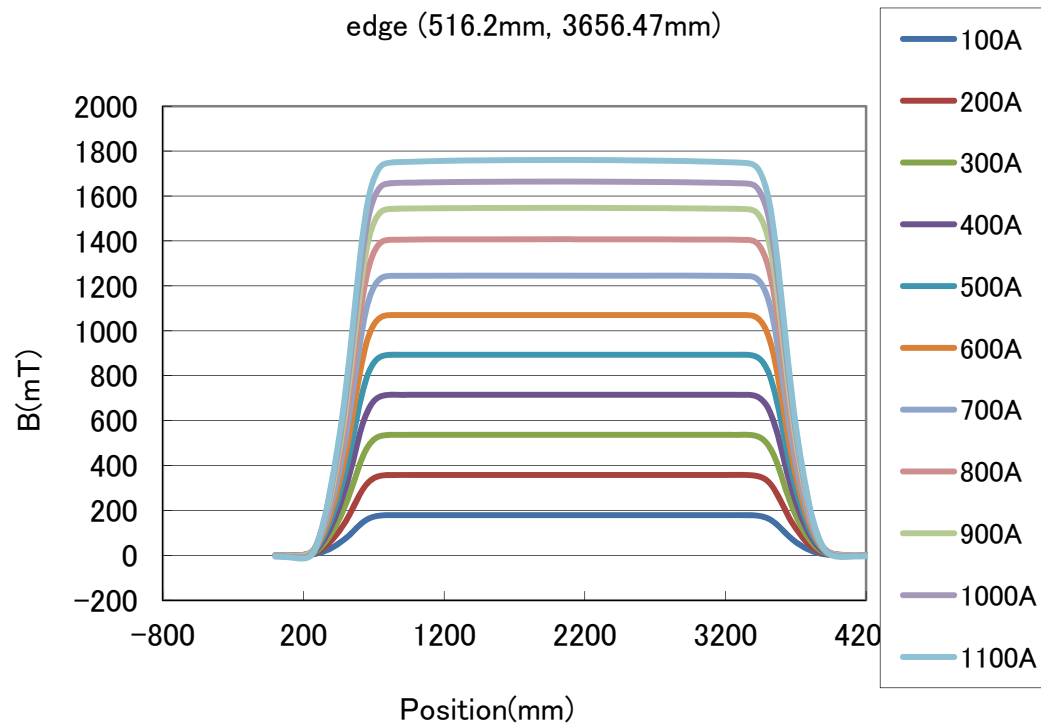


Dipole map



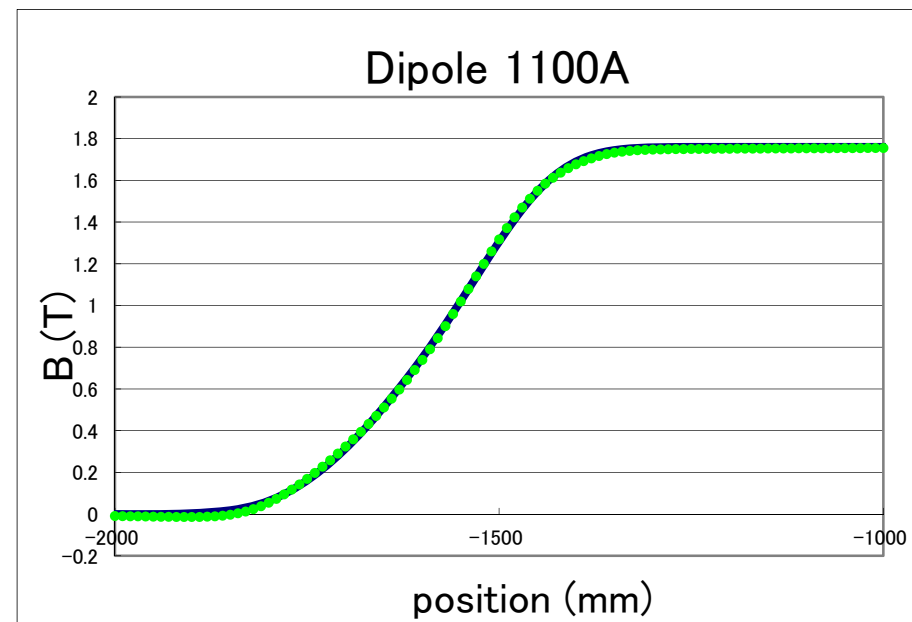
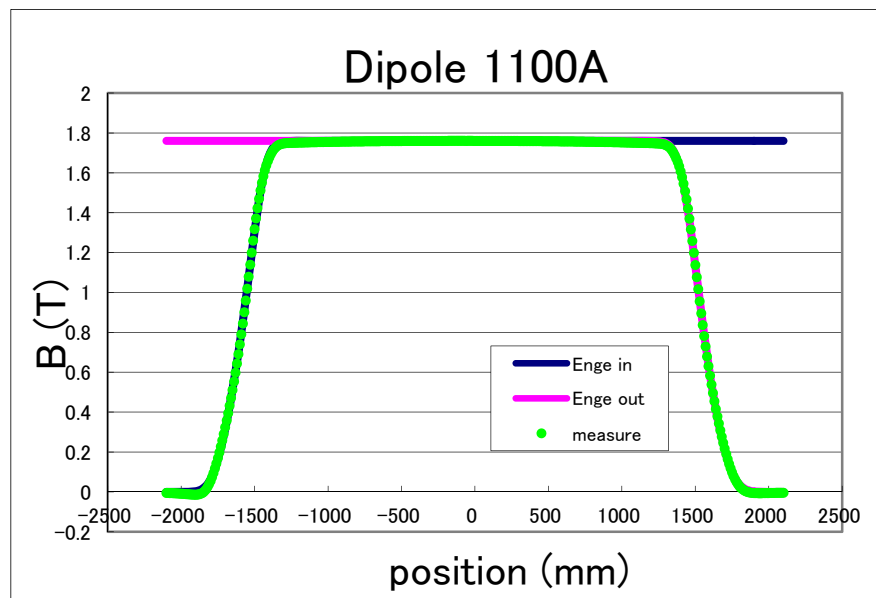
1100A

edge (516.2mm, 3656.47mm)



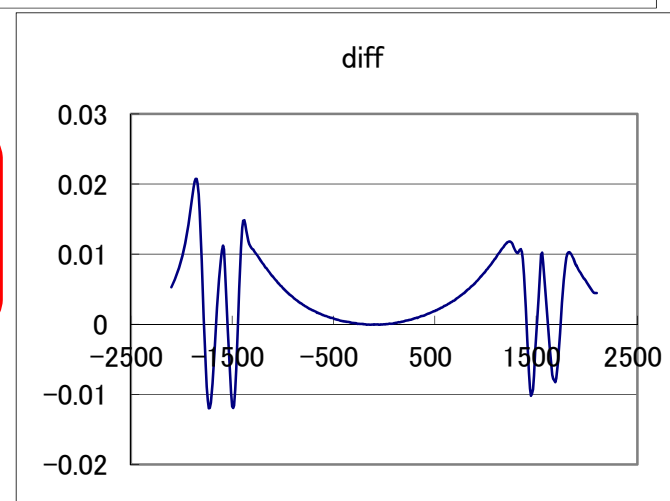


Fitting by Enge function



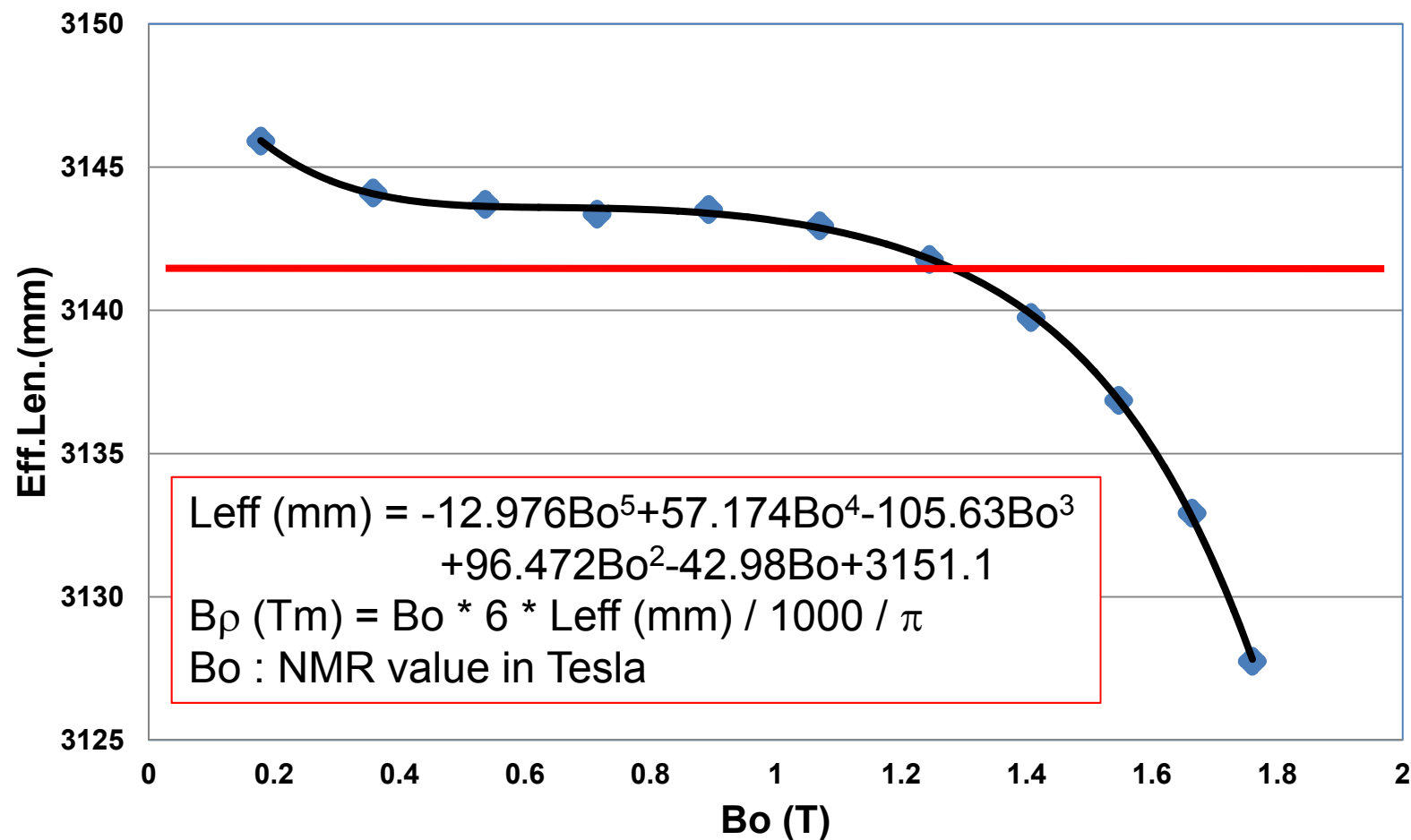
$$F(z) = \frac{1}{1 + \exp \left[a_1 + a_2 \left(z/D \right) + \dots + a_6 \left(z/D \right)^5 \right]}$$

→ implemented in COSY





Effective length of dipole



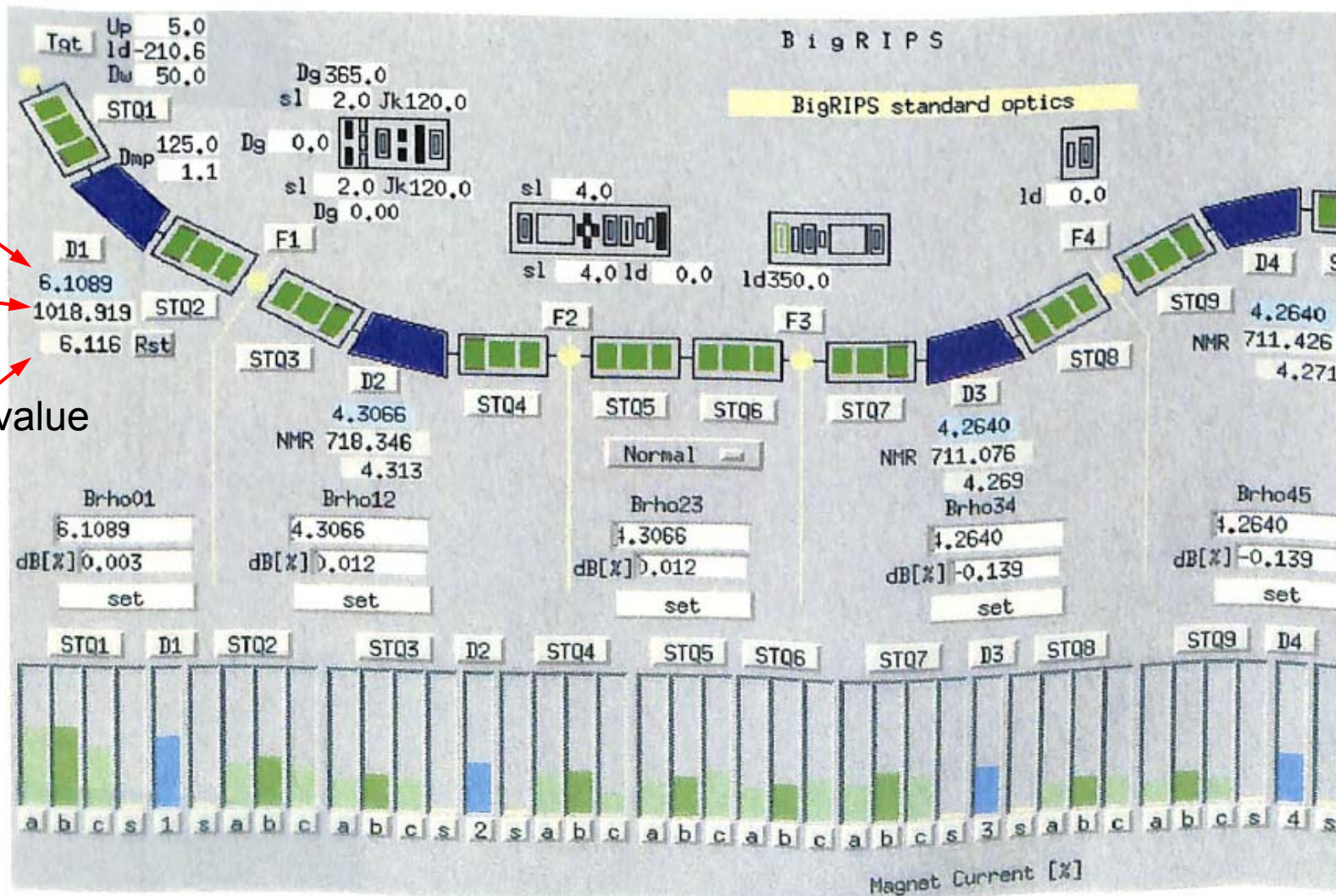
B_ρ correction by effective length is important for absolute value determination of A/Q



B_p set value

NMR value

corrected B_p value



Magnet current settings for STQ

Set $B\rho \rightarrow$ field strength (B_{COSY}) \rightarrow set current (I_{COSY})

\uparrow COSY fitting \uparrow B-I curve

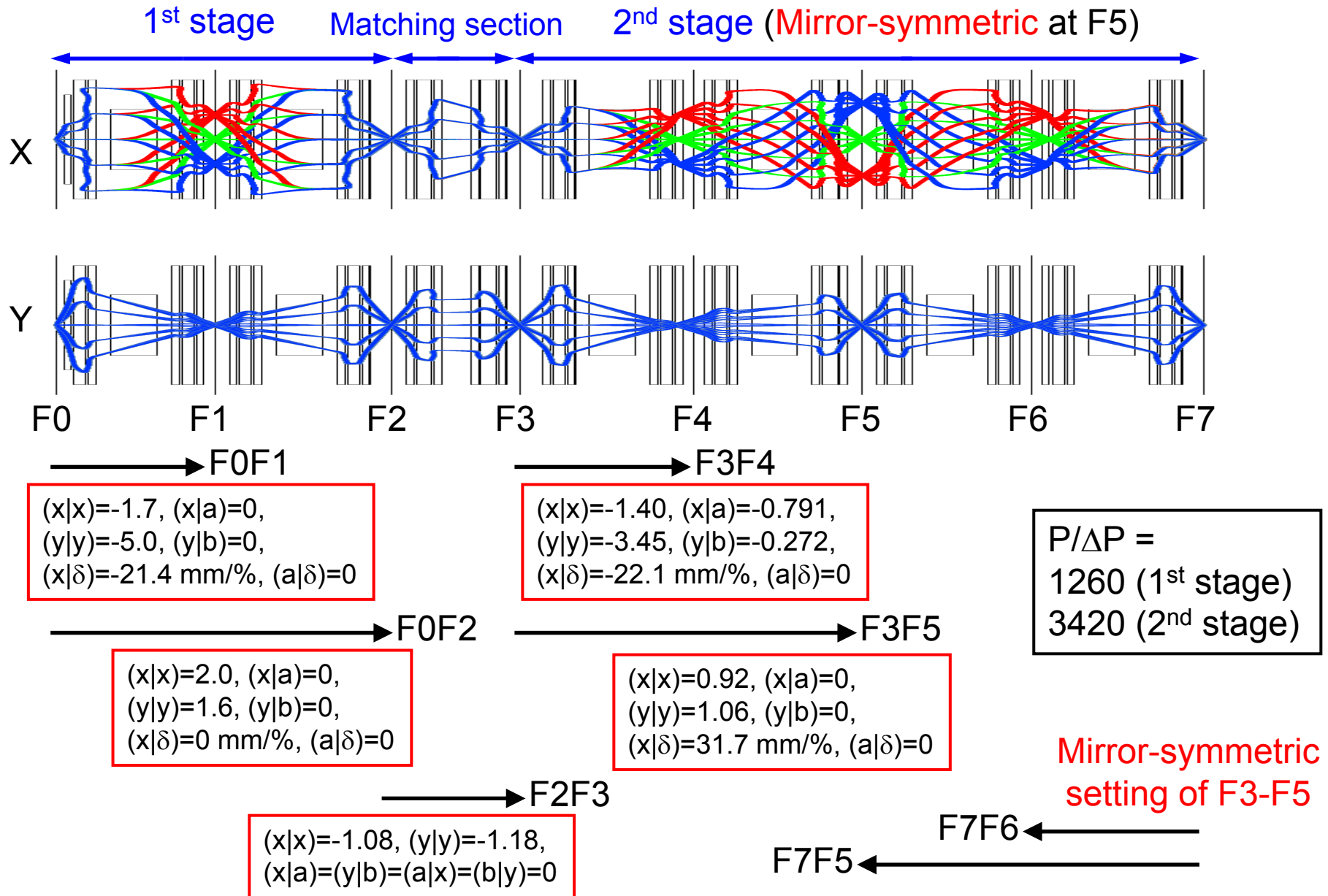
Repeat in 0.5Tm steps to find $B\rho$ -B function for each quadrupole. These functions are prepared for each optical mode. B-I curves are implemented in magnet control system (EPICS). Thus currents of all magnets are set by just putting $B\rho$ value.

Quality of $B\rho$ -B function is very important.

Sometimes $B\rho$ -B function results in uneven behavior, which causes unexpected optical conditions (out of focus, etc).

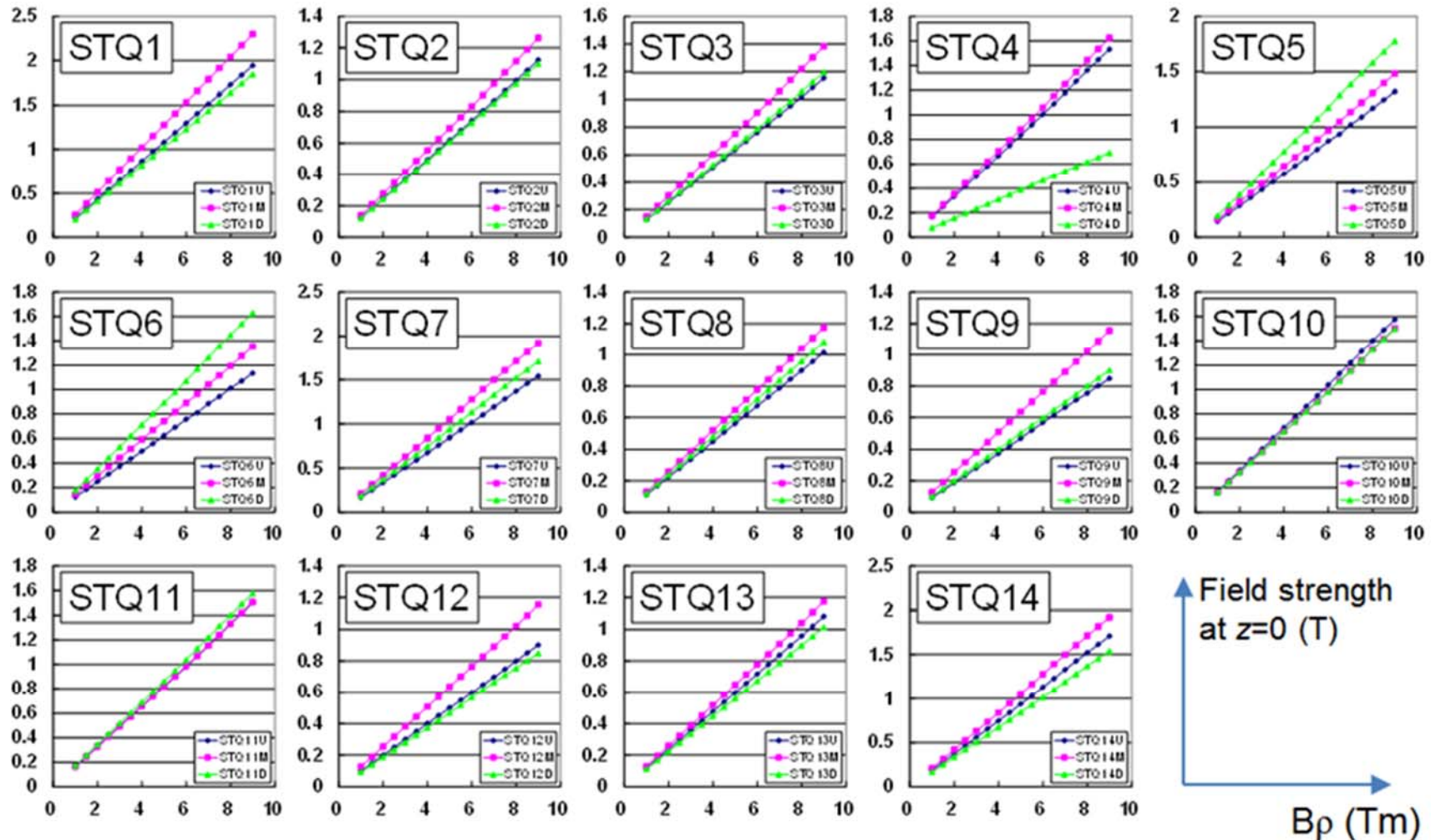
Disagreement between experiment and COSY becomes large in such cases.

Required conditions for the standard BigRIPS mode



Field strengths of the three quadrupoles in each STQ

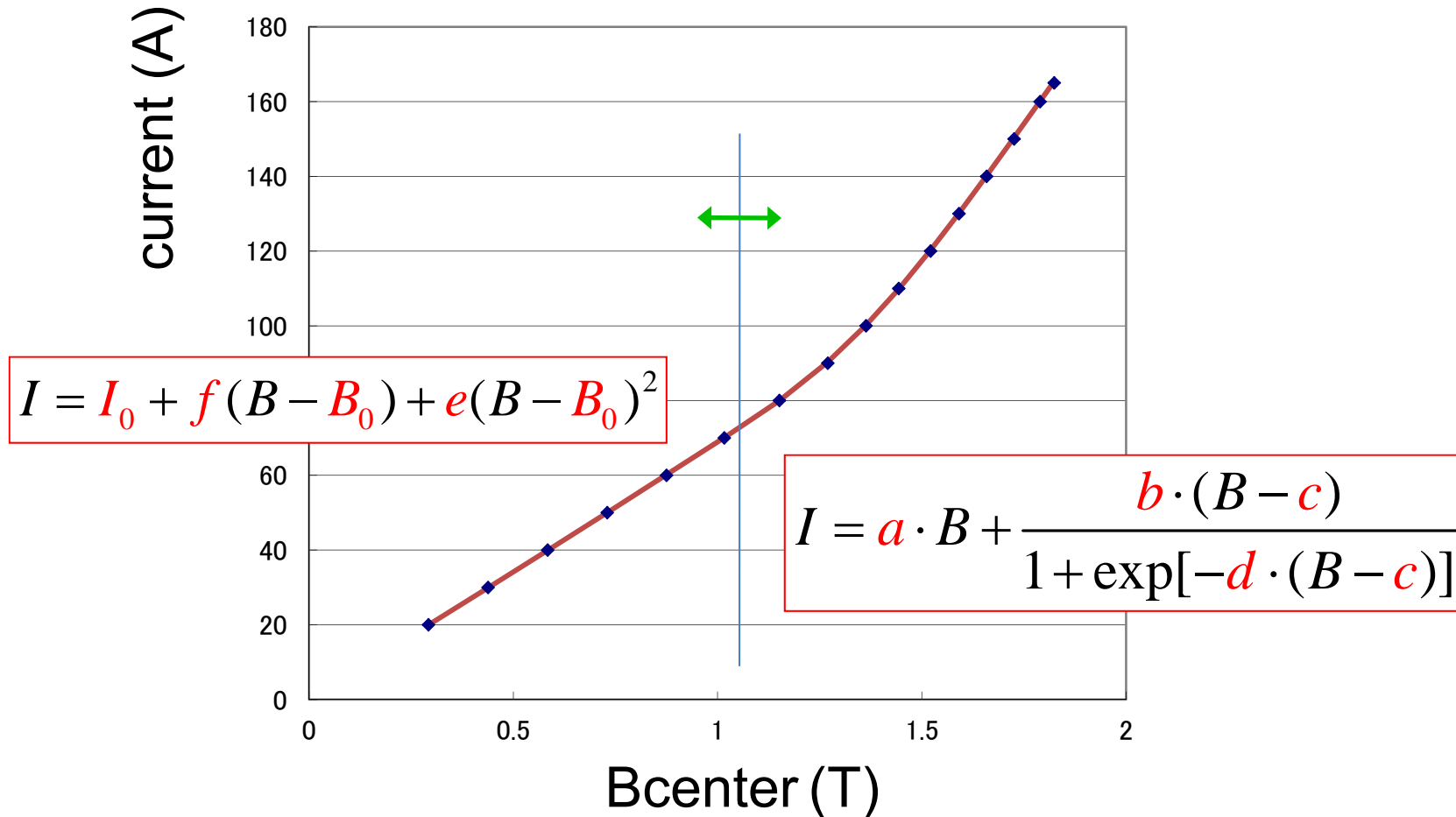
(BigRIPS standard mode)



Slope and offset parameters are implemented in the magnet control system (EPICS)

B-I curve

Q500

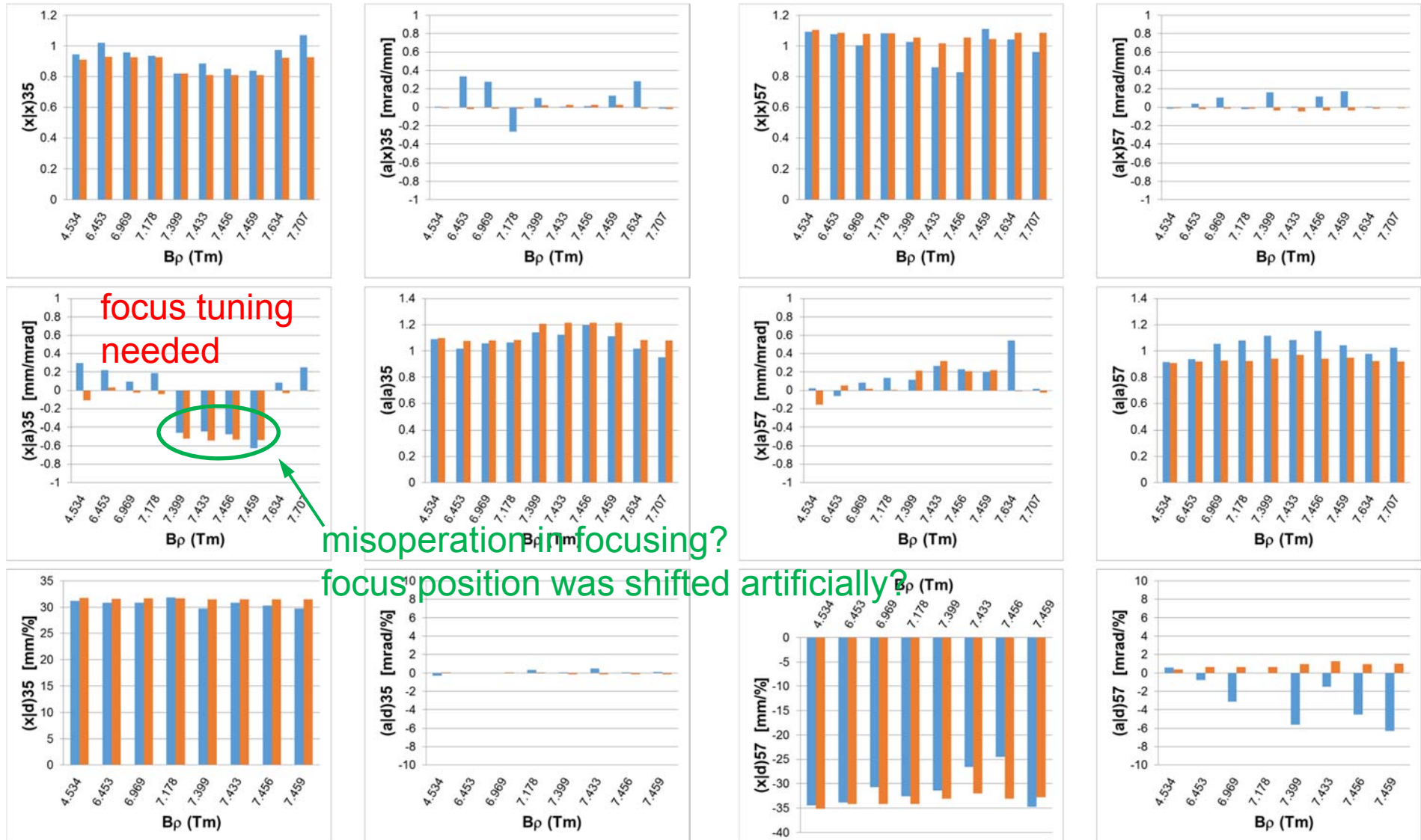


- same for other super-ferric quadrupoles and dipoles
- linear functions are used for air-core quads

Transfer matrix elements

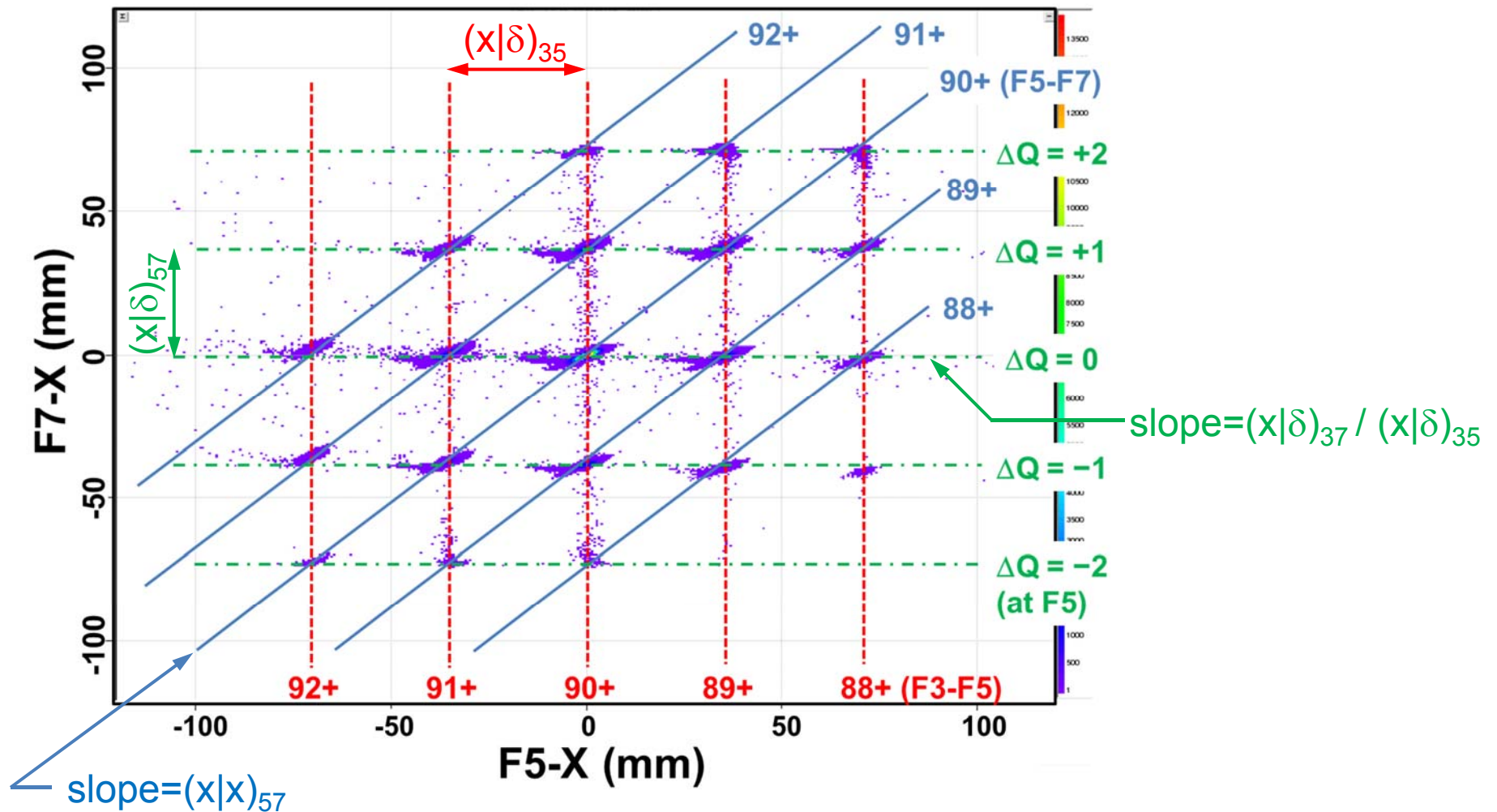
F3-F5

F5-F7

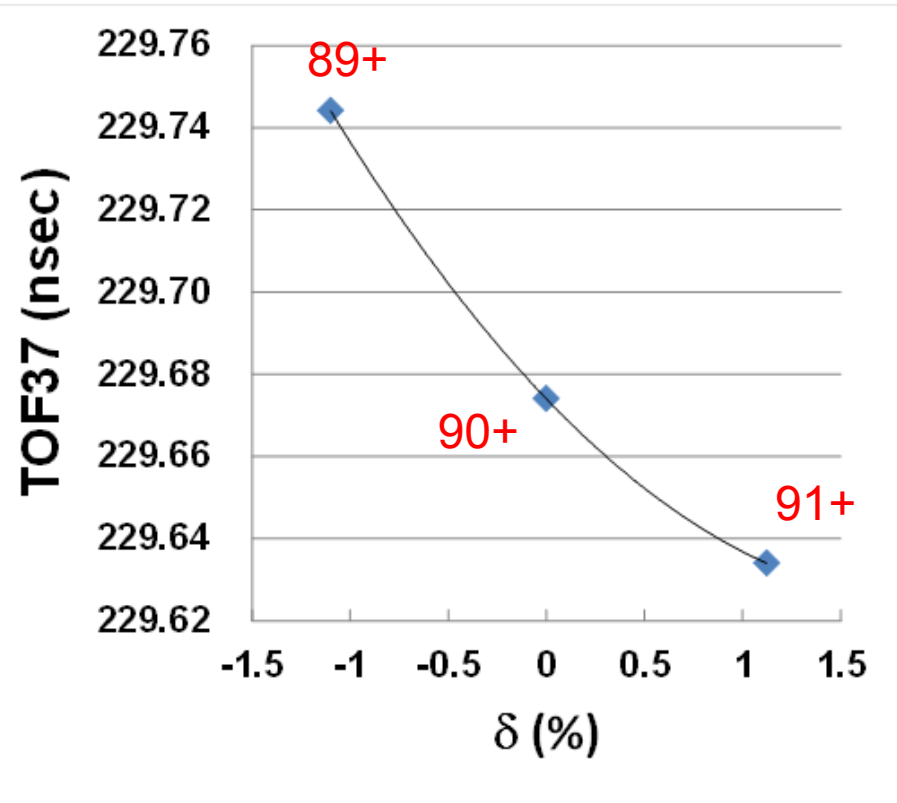


■ measured ■ COSY

transfer matrix measurement with ^{238}U primary beam



$(L|\delta)$ measurement with primary beam



All the charge states have the same velocity.
Flight-path-length difference can easily be deduced by the TOF measurements.

$$\begin{aligned}(\text{TOF}|\delta) &= -0.0498\text{ns}/\% \\ \rightarrow (L|\delta) &= -10.2\text{mm}/\% \\ (\text{COSY}) &= -6.5\text{mm}/\%\end{aligned}$$

Summary & Issues

- Large aperture, short length, strong field magnets are used in BigRIPS
- 3D magnetic field is successfully extracted from 2D surface data on a cylinder
 - quadrupole and higher multipoles
- successfully applied to ion-optics of BigRIPS
- room for further improvement in focusing
- similar procedure for dipole?
 - curved reference orbit